JOURNAL OF MATERIALS SCIENCE 21 (1986) 3901–3906

Interparticle welding, mechanical properties and fracture behaviour of $LaCrO_3$–Cr cermets

YU. L. KRASULIN, S. M. BARINOV, V. S. IVANOV
Academy of Science of the USSR, Baikov Institute of Metallurgy, Moscow, USSR

The temperature dependence of strength, fracture toughness, work-of-fracture and creep rate of $LaCrO_3$–Cr cermets has been studied. The influence of structure formation conditions on mechanical properties was also investigated. The best results have been obtained for cermets made under conditions of restricted volume interaction of constituent phases. The mechanical properties are discussed in terms of energy dissipation in the crack tip zone.

1. Introduction

The mechanical properties of refractory oxide–metal cermets are governed by the volume content, distribution and dispersity of components, the porosity of materials and the interparticle boundary state [1, 2]. It is important to realize the attractive properties of both metallic and ceramic phases in compact material. The sintering process leads to recrystallization, and to formation of brittle intermediate grain-boundary phases. As a consequence, the mechanical properties of sintered cermets are far from the desired level. The fracture of materials is brittle and intergranular, the fracture toughness is low. For the reliable performance of brittle materials it is important to guarantee the possibilities of elastic strain energy relaxation prior to the onset of unstable fracture. The possible mechanisms of strain energy relaxation in cermets are subcritical crack growth, and plastic deformation of the metallic phase induced around the crack tip. It is possible to realize the latter process if the metallic phase is plastic and can be involved in the deformation process. The development of such processes generally increases the fracture toughness of the material. Plastic deformation is possible only if the bond between the metallic and oxide phases is strong and mass-transport processes are limited during consolidation of the particles as has been mentioned above. The high-speed method of compacting provides interaction of powder particles, as in the case of interparticle welding with strong bonding of particles [3–5]. This method was applied successfully to different materials including metals, alloys and ceramics [3–10]. In this paper the results of investigation of the mechanical properties of dynamically compacted $LaCrO_3$–Cr cermets are described and discussed with special attention to non-linear fracture behaviour.

2. Experimental procedure

The 60 wt % $LaCrO_3$–40 wt % Cr cermets were obtained by sintering after quasistatic pressing (SC) and high-speed pressing (HPC). Details of such processes have been given earlier [3, 6, 11]. The porosities of HPC and SC were about 4 and 8%, respectively.

The mechanical properties: modulus of rupture (bending strength) σ_b, deformation at fracture ε_b, stress intensity factor K_{Ic} and work-of-fracture γ_F, were estimated in the temperature range 20 to 1200° C by three-point loading of rectangular 3 mm × 6 mm × 40 mm bars in an argon-filled furnace type Ta 1028 at a transverse travel speed of 8×10^{-6} m sec^{-1}. The testing machine was an Instron 1115. For correct σ_b and ε_b determinations the non-linearity of the deformation diagrams was taken into consideration by [12]:

$$\sigma_b = \frac{3PL}{2bh^2}\frac{2+\mu}{3}, \quad (1)$$

$$\varepsilon_b = \frac{4h\delta}{L^2}\frac{2\mu+1}{\mu+1}, \quad (2)$$

where P and δ are the load and deflection, b and h are the width and height of the bar, L is the span, μ is the non-linearity coefficient of the stress–strain diagrams. The stress intensity factor K_{Ic} was determined using a common technique provided that the correction condition $P_{max}/P_Q \leqslant 1.1$ is satisfied [13]. The depth of the notch in the specimens was $0.5h$, and the radius of curvature of the notch tip was about 50 μm. The work-of-fracture, γ_F was determined as the ratio of total deformation work of the notched beam to the doubled fracture surface area. K_{Ic} and γ_F were determined, on average, from three to five specimens. The relative error of the strength and fracture toughness measurements was estimated as 17% and 15%, respectively. The creep of HPC and SC specimens was investigated by four-point bending in the temperature range 1250 to 1450° C and stress levels of 1, 2 and 4 MPa.

The thermal shock fracture resistance test was performed using cylindrical specimens 10 mm diameter and 20 mm long. The ratio of compressive strength of specimens after thermal shock 20–1350–20° C to control (unshocked) specimens strength was determined. The number of thermal cycles was up to 50.

Scanning electron microscopy (SEM) was used to investigate the interparticle bonding during structure formation.

3. Results

Fig. 1 is an optical micrograph of HPC and SC

0022–2461/86 $03.00 + .12

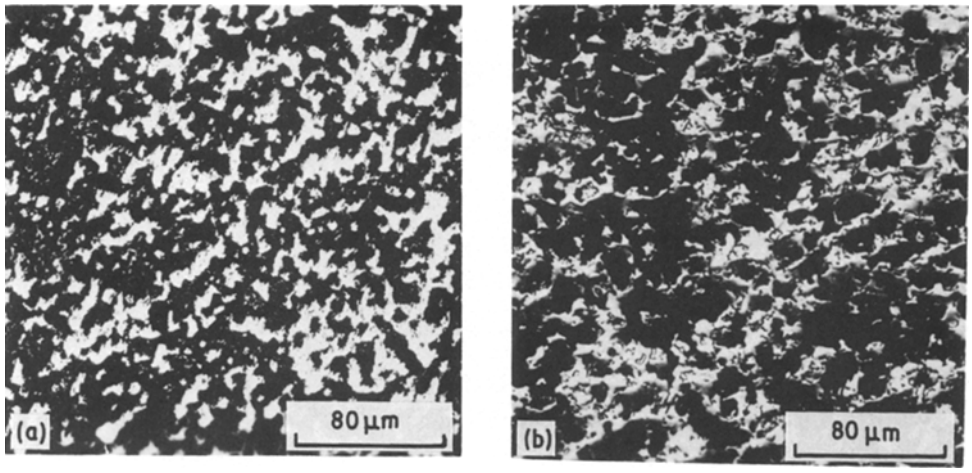

Figure 1 Structures of (a) HPC and (b) SC specimens.

specimens. It is evident that the particle distribution in HPC is more uniform than in SC. Both metallic and oxide phases form interpenetrating continuous frameworks. Fig. 2 shows SEM fractographs of the room-temperature ruptured HPC specimens before and after heat treatment at different temperatures. The fracture mode changes from fully intergranular to mixed trans- and intergranular with increasing heat-treatment temperature. The compressive strength of the green compact HPC is 110 MPa and increases with heat-treatment temperature. These results indicate that interparticle bonding forms on the compacting stage and develops during heat treatment.

Fig. 3 shows the temperature dependencies of σ_b and ε_b. The strength decreases and the strain increases with temperatures above 700° C. Deformation of notched SC specimens is linear-elastic up to unstable fracture. Notched specimens of HPC have a non-linear deformation stage even at room temperature (Fig. 4). To ascertain the nature of the non-linearity, experiments were performed with repeated loading–unloading during the deformation process. It was concluded that residual deformation is caused by plastic deformation of the metallic phase at slow crack extension.

The dependencies of K_{Ic} and γ_F upon temperature are shown in Fig. 5. The increase of K_{Ic} and γ_F begins at 500° C. K_{Ic} reaches a maximum at 500° C and then decreases. All mechanical properties of HPC are higher than those of SC.

Thermal shock fracture resistance data are given in Table I. The relative retained strength of HPC is much higher than that of SC.

Figs 6 and 7 are the dependencies of steady-state creep rate $\dot{\varepsilon}$ on temperature and applied stress. It can be seen that the creep rate of HPC exceeds that of SC at the same temperatures, T, and stresses, σ. The mean slope angle tangent of $\lg \dot{\varepsilon}$–$\log \sigma$ is about 1. Then the $\dot{\varepsilon} = \dot{\varepsilon}(T, \sigma)$ dependence can be written as

$$\dot{\varepsilon} = A\sigma \exp(-Q/kT) \quad (3)$$

where A and k are constants, and Q is the apparent activation energy. From the slope of the $\lg \dot{\varepsilon}$–$1/T$ curves one can estimate Q. Its average value in the T and σ range investigated is about 314 kJ mol^{-1}.

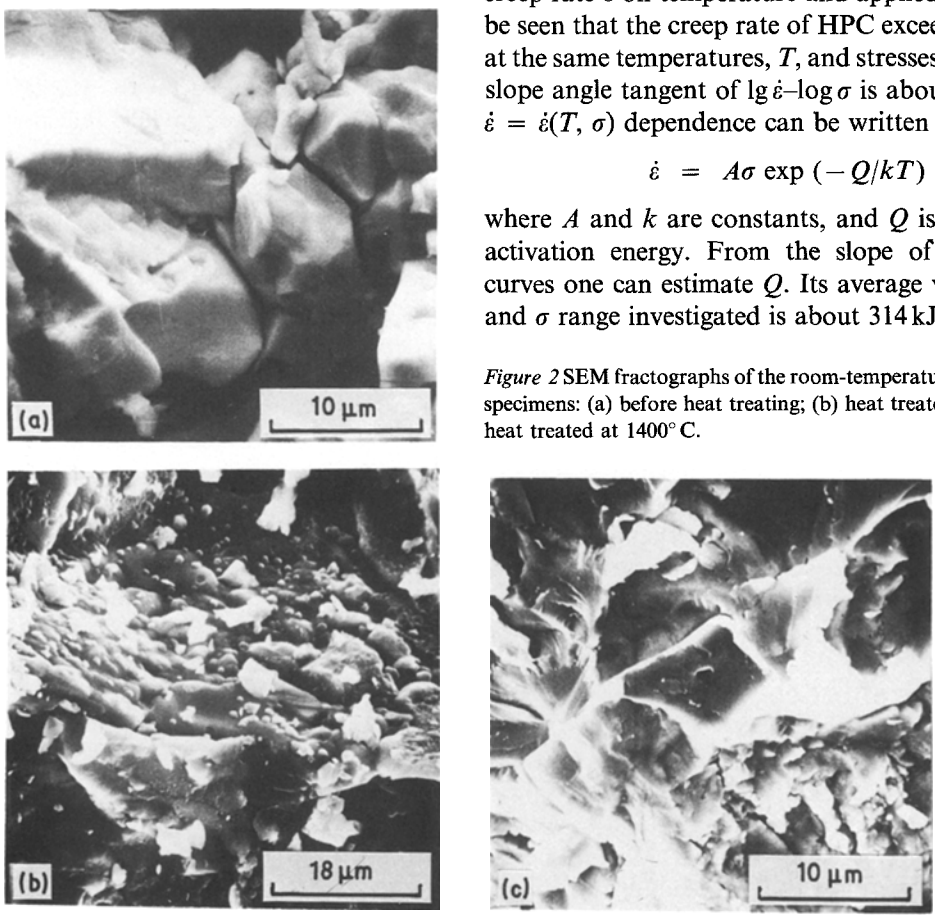

Figure 2 SEM fractographs of the room-temperature ruptured HPC specimens: (a) before heat treating; (b) heat treated at 1000° C; (c) heat treated at 1400° C.

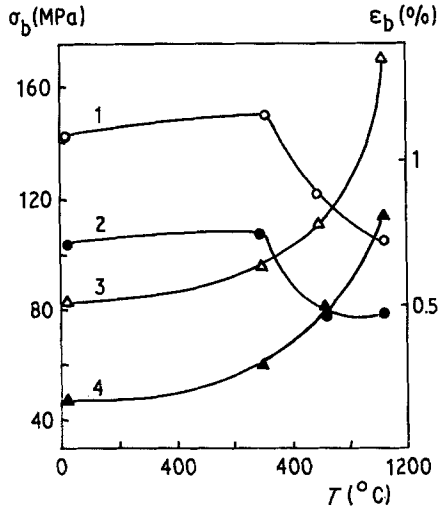

Figure 3 Temperature dependence of σ_b (1, 2) and ε_b (3, 4) of HPC (1, 3) and SC (2, 4).

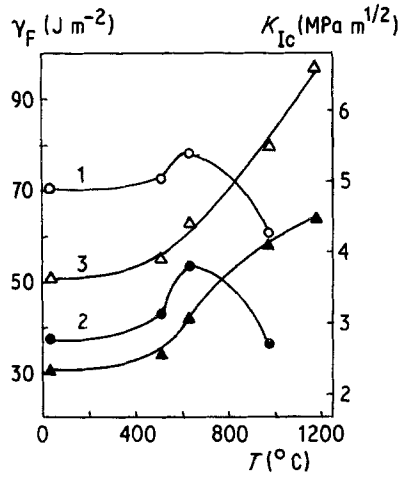

Figure 5 Temperature dependence of K_{Ic} (1, 2) and γ_F (3, 4) of HPC (1, 3) and SC (2, 4).

4. Discussion

4.1. Structure formation

As has been shown in recent investigations, (see, for example, [3–5]), high-speed compacting results in a more effective consolidation of powder particles because of interparticle welding with self-cleaning of the particle surfaces and high-temperature local heating. Local heating is caused by adiabatic compression, interparticle friction and plastic deformation. The heating of the particle surface regions reaches temperatures which are much higher than the mean body temperature, up to melting point [14, 15]. Surface regions then cool rapidly ($> 10^5$ K sec^{-1} [6, 14]). As a result, the particles are welded and zones of particles with defect structure form [3–6, 14, 15].

The green strength value of HPC indicates that interparticle interaction zones have formed during the pressing process. Some such zones can be seen on the fracture surfaces of HPC specimens in Fig. 2. With increasing heat-treatment temperatures, the density and area of interparticle interaction zones will increase. The fracture mode changes from intercrystalline to mixed trans- and intercrystalline. Local X-ray analysis shows that in heat-treated HPC specimens extended interparticle zones with a graded profile of chromium concentration may be found. This fact indicates a diffusion of chromium into the $LaCrO_3$ grains. In SC specimens the chromium concentration profile is sharp at the intergrain zone. Apparently, the development of the diffusion proceses in HPC is due to higher atomic and linear density, and structure instability near the interparticle contacts in HPC specimens.

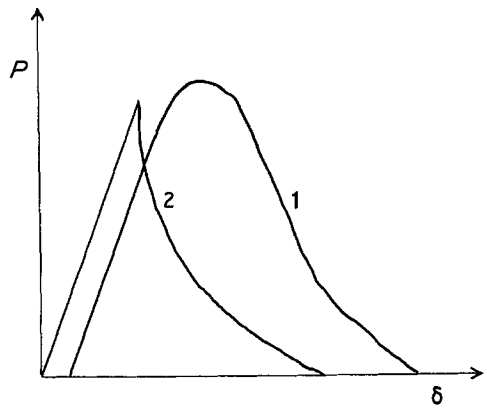

Figure 4 The deformation diagrams of notched HPC (1) and SC (2) specimens.

The microstructure of HPC has some peculiarities. Fine substructure formation and particle cracking can occur. Correlation of these processes depends upon the interatomic bond in the sustance. Electron microscopy investigations indicate that in the high-speed compacting process, cracking of the $LaCrO_3$ grains occurs. X-ray diffraction measurements have shown that the diffraction lines of both chromium and chromite phases are broadened. These facts indicate that the structure of the material is stressed and fractionated. The increased dislocation density in shock-treated ion-covalent crystals was established by Skorochod *et al.* [16]. The high dislocation density in the oxide phase of cermet can appear as a result of brittle–ductile transition under conditions of high pressure and temperature development during compaction. Measurements of X-ray diffraction line broadening shows that the substructure formed is thermally stable up to 1500° C.

4.2. Mechanical properties and fracture

The values of strength, deformation at failure, critical stress intensity factor and work-of-fracture of HPC exceed those of SC specimens. There are two effects that can be taken into account to explore this fact. The first is the porosity difference of the cermets, and the second is the difference in interparticle bonding effectivity.

According to Ryshkevitch's formula [17]

$$\sigma_b = \sigma_{b0} \exp(-c\theta), \quad (4)$$

where σ_{b0} is the strength of body without pores, c is an

TABLE I Relative retained compressive strength after thermal shock

Cermets	$(\sigma/\sigma_0) \times 100\%$*	
	after 20 cycles	after 50 cycles
HPC	70	65
SC	30	16

*σ is the strength after cycling, σ_0 is the strength of the control sample.

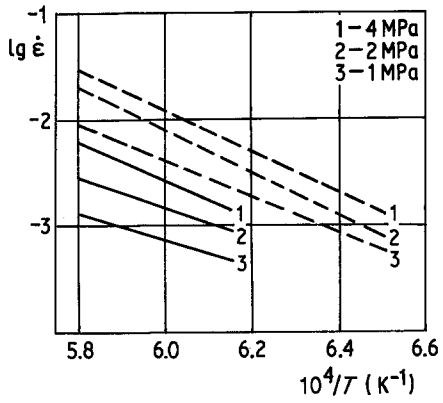

Figure 6 Steady-state creep rate (h^{-1}) dependence of HPC (dashed lines) and SC (solid lines) on temperature.

empirical constant and θ is the volume pore content. The estimates show that the porosity is not the only effect concerned, because the ratio between HPC and SC strength is higher than the Ryshkevitch formula predicts.

The increased K_{Ic} value of HPC is the result of higher strength and slow crack extension (see Fig. 4). The subcritical slow crack extension occurs at temperatures below 1100° C only in HPC specimens. Slow crack growth is due to relaxation zone formation and extension near the crack tip. In cermets, two mechanisms can be taken into consideration for stored elastic energy relaxation. The first is the metallic phase microplastic deformation, the second is microcracking ahead of the crack tip. Nevertheless, the description of fracture development in both cases is formally similar.

The model of slow crack growth under conditions of continuous loading can be used as a basis for discussion [18]. The energy balance equation can be written as

$$2\gamma\delta l = \delta A_e + \delta A_r, \tag{5}$$

where δl is the crack length increment, δA_e is the value of releasing elastic strain energy at the constant relaxation zone parameter r, δA_r is the value of energy relaxation in the relaxation zone while increasing r from r to $r + \delta r$. δA_e is [18]:

$$\delta A_e = \alpha_1(K_I^2/E)\delta l, \tag{6}$$

where α_1 is a constant, E is the elasticity modulus. δA_r is proportional to the relative density ϱ_r, of relaxation sites, to $r\delta r$ and to specific work a_r of relaxation. As has been shown [19, 20], the zone parameter r can be written as

$$r = \alpha_2(K_I/\sigma_i)^2 \tag{7}$$

where σ_i is the yield stress, σ_y, of the metallic particulate phase in the case of microplastic deformation or the fracture stress, σ_F, in the case of microcracking. The value of α_2 in Equation 7 also depends on the relaxation mechanism.

No evidence of microcracking has been obtained by structural investigation of cermet fracture surfaces.

It it is assumed that microplastic deformation is responsible for the subcritical crack growth, then two conditions must be satisfied, namely, plasticity of chromium particles and a strong bonding of metal and ceramic phases [21]. It is known that the brittle–ductile transformation temperature decreases with diminishing of chromium grain size [22]. The high-speed compaction of cermets results in fragmentation of the chromium particle structure, as has been shown by X-ray diffraction. High-speed compaction also leads to interparticle welding, reduced porosity and, hence, to reduced stress concentration. As a result, the material can be obtained with a metallic phase which can be deformed plastically. This condition is satisfied only in HPC.

The value δA_r in Equation 5 can be expressed as

$$\delta A_r = (\varrho_r/\varrho_0)a_r r\delta r, \tag{8}$$

where ϱ_0 is a number of potential relaxation sites in a relaxation zone ahead of the crack tip. In a stiff-plastic body approximation for the metallic phase, the a_r value can be evaluated as

$$a_r = \sigma_y\varepsilon, \tag{9}$$

where ε is the deformation. As a result of combining Equations 6, 8, 9 and 5 we obtain

$$\gamma = \alpha_1 K_I^2/2E + \alpha_2^2\varrho_r\varepsilon(K_I/\sigma_y)^3(\delta K_I/\delta l) \tag{10}$$

if condition $\varrho_0 \to 1$ is satisfied.

Taking into account that $\gamma = \alpha_1 K_{Ic}^2/2E$, where K_{Ic} is the critical stress intensity factor, we can obtain from Equation 10

$$\frac{dl}{dK_I} = \frac{2\alpha_2^2}{\alpha_1}\varrho_r\varepsilon E K_I^3/\sigma_y^3(K_{Ic}^2 - K_I^2) \tag{11}$$

Integration of Equation 11 results in

$$\Delta l = l - l_0 = \left(\frac{\alpha_2}{\alpha_r}\right)\left(\frac{\varrho_r\varepsilon E r_c}{\sigma_y}\right)\left\{\left(\frac{K_I}{K_{Ic}}\right)^2 + \ln\left[1 - \left(\frac{K_I}{K_{Ic}}\right)^2\right]\right\} \tag{12}$$

where $r_c = \alpha_2(K_{Ic}/\sigma_y)^2$ is the critical zone size parameter. The dependence of K_I/K_{Ic} on Δl^* is shown in Fig. 8, where Δl^* is $\Delta l/(\alpha_2/\alpha_1)(\varrho_r\varepsilon E r_c/\sigma_y)$. The instability of the crack begins when $\Delta l^* > 1$. According to this the higher the value of $(\alpha_2/\alpha_1)(\varrho_r\varepsilon E r_c/\sigma_y)$ the more extended is the slow crack growth. Therefore, a cermet able to store energy relaxation by slow crack growth must have a metallic phase with a low yield stress and high deformability. In HPC the metallic phase is fragmented and strongly bonded to the oxide phase. As a result the enhanced relaxability of the cermet is attained.

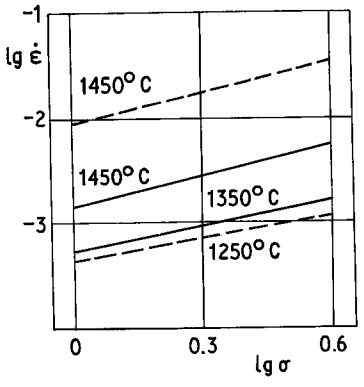

Figure 7 Steady-state creep rate (h^{-1}) dependence of HPC (dashed lines) and SC (solid lines) on applied stress.

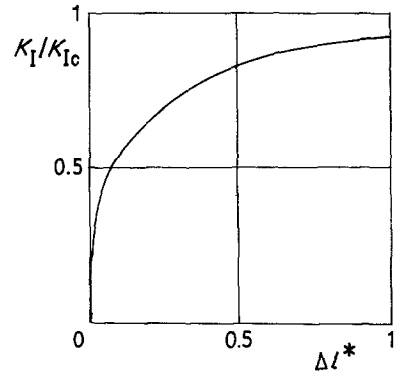

Figure 8 Independence of K_I/K_{Ic} and normalized crack extension Δl^*.

Since slow crack extension is more pronounced in HPC, a rising crack growth resistance curve would cause the computed K_{Ic} to increase with respect to SC. This is in agreement with the results shown in Fig. 6. The increase of γ_F values in HPC with respect to those in SC is due to slow crack growth and more stable fracture after maximum load. The increase of γ_F with temperature is a result of increasing plasticity. At the same time, the decrease of K_{Ic} is due to diminishing yield stress of the cermets because deformation of cermets takes place without work-hardening.

The thermal shock fracture resistance of cermets varies with respect to the difference of their strength and fracture toughness. Estimates of the thermal shock fracture resistance parameters are given in Table II, where $R = \sigma_b/E\alpha$, α is the thermal coefficient of expansion, P_1 and P_2 are the fracture loads of notched and unnotched specimens, respectively, and l is the notch depth. The ratio $(P_1/P_2)^2 l$ is proportional to the R^{IV} criterion of thermal shock fracture [23].

The results given in Table II agree with the strength deterioration measurement results after thermal shock as one can see in Table I. The HPC specimens have both higher crack initiation and crack propagation resistance at thermal shock.

4.3. Creep

The apparent creep activation energy in both HPC and SC is nearly equal to the chromium self-diffusion energy [24]. This value would be expected to correspond to the volume diffusion mechanism of creep in the chromium skeleton. But it is evident from the structure investigation, that the continuous skeleton is formed by oxide phase. Therefore, it would be anticipated that the creep rate of cermets is limited by the rate of surface diffusion in the oxide component.

The major difference between creep of HPC and SC is that the creep rate of the former is much higher than the latter. This fact can be explained by the structure development of HPC. The grain-boundary diffusion creep rate of material with equilibrium structure is governed by the size of a structural unit, L, and the grain-boundary diffusion coefficient, D_{gb}:

$$\dot{\varepsilon} \sim A\sigma D_{gb}/L^3 kT, \quad (13)$$

where A is a constant. The HCP structure is fragmented as a consequence of substructure formation and particle cracking, as has been shown by X-ray diffraction measurements and TEM investigations. Hence, according to Equation 13, the creep rate of HPC must be enhanced. This conclusion is suggested by the creep-test results of HPC after heat treatment that increases the subgrain size [25]. As a result, the creep rate of HPC has been decreased.

TABLE II Thermal shock fracture parameters of cermets

Cermets	R (° C)		$(P_1/P_2)^2 l$ (mm)	
	at 20° C	at 700° C	at 20° C	at 700° C
HPC	648	670	0.54	1.03
SC	246	314	0.18	0.24

5. Conclusions

The mechanical behaviour of the $LaCrO_3$–Cr cermets investigated depends on structure peculiarities. The cermets obtained under interparticle welding conditions, with restricted volume interaction of components, have preferable properties. The main advantage of HPC is the rising crack resistance curve causing the enhanced fracture toughness and thermal shock fracture resistance. The structure fragmentation of such cermet leads to an increased creep rate and consequently to higher relaxability.

Acknowledgements

The authors are particularly grateful to Dr E. S. Atroshenko for his help in specimen preparation and to Dr V. S. Bakunov for creep testing.

References

1. J. R. TINKLEPAUGH and W. D. CRANDALL, "Cermets" (Reinhold, New York, 1960).
2. P. S. KISLIJ, in "Encyclopedia of inorganic materials", Vol. 1 (Ukrainskaja Sovetskaja Enciclopedija, Kiev, 1977) p. 565.
3. YU. L. KRASULIN, V. S. IVANOV and S. M. BARINOV, in "Grundlagen, Herstellung und Eigenschaften pulvermet. Wekstof", Vol. 3 (Dresden, 1981) p. 63.
4. D. RAYBOULD, *J. Mater. Sci.* **16** (1981) 589.
5. S. M. BARINOV, V. S. IVANOV and YU. L. KRASULIN, *Phys. Chem. Materials Treatment* (*USSR*) **2** (1984) 118.
6. M. A. MYERS, B. B. GUPTA and L. E. MURR, *J. Metals* **10** (1981) 21.
7. O. R. BERGMANN and J. BARRINGTON, *J. Amer. Ceram. Soc.* **49** (1966) 502.
8. M. MITOMO and N. SETAKA, *J. Mater. Sci.* **16** (1981) 851.
9. R. PRUEMMER and G. ZIEGLER, *Powder Met. Int.* **9** (1977) 11.
10. A. K. BHALLA and J. D. WILLIAMS, *Powder Met.* **19** (1976) 31.
11. E. S. ATROSHENKO, B. M. BARYKIN, V. S. IVANOV, YU. L. KRASULIN and E. G. SPIRIDONOV, *High Temp. High Press.* **8** (1976) 21.
12. S. M. BARINOV, *Zavodskaja Laboratorija* (*USSR*) **48** (1982) 78.
13. P. G. MIKLAEV, G. S. NESHPOR and V. G. KUDRJASHOV, "Fracture Kinetics" (Metallurgija, Moscow, (1979).
14. D. G. MORRIS, *Metal Sci.* **16** (1982) 457.
15. *Idem, J. Mater. Sci.* **17** (1982) 1789.
16. V. V. SKOROCHOD, G. I. SAVVAKIN and S. M. SOLONIN, *Powder Met.* (*USSR*) **8** (1974) 80.
17. E. RYSHKEVITCH, *J. Amer. Ceram. Soc.* **36** (1953) 65.
18. G. R. CHEREPANOV, "Mechanics of Brittle Fracture" (Nauka, Moscow, 1974).

19. S. M. BARINOV and YU. L. KRASULIN, *Strength problems* (*USSR*) **9** (1982) 84.
20. S. M. BARINOV, YU. L. KRASULIN and V. S. IVANOV, in Proceedings of the VI International Powder Metallurgy Conference in ČSSR, Vol. 2 (Brno, 1982) p. 189.
21. V. V. KRISTIČ, P. S. NICHOLSON and R. C. HOAGLAND, *J. Amer. Ceram. Soc.* **64** (1981) 499.
22. V. I. TREFILOV, YU. V. MILMAN and S. A. FIRSTOV, "Physics of Refractory Metals Strength" (Naukova Dumka, Kiev, 1975).
23. S. M. BARINOV and YU. L. KRASULIN, *Zavodskaja Laboratorija* (*USSR*) **48** (1982) 62.
24. C. J. SMITHELLS, "Metals Reference Book" (Butterworths, London, Boston, 1976).
25. S. M. BARINOV, V. S. BAKUNOV, V. S. IVANOV, YU. L. KRASULIN and E. G. SPIRIDONOV, *Phys. Chem. Materials Treatment* (*USSR*) **3** (1983) 154.

Received 28 May 1985
and accepted 21 January 1986